Hybrid thin films derived from UV-curable acrylate-modified waterborne polyurethane and monodispersed colloidal silica

W. C. Lin[1], C. H. Yang[2], T. L. Wang[2], Y. T. Shieh[2], W. J. Chen[2]*

[1]Department of Environmental Engineering, Kun Shan University, Tainan 710, Taiwan
[2]Department of Chemical and Materials Engineering, National University of Kaohsiung, Kaohsiung 811, Taiwan

Abstract. Hybrid thin films containing nano-sized inorganic domains were synthesized from UV-curable acrylate-modified waterborne polyurethane (WPU-AC) and monodispersed colloidal silica with coupling agent. The coupling agent, 3-(trimethoxysilyl)propyl methacrylate (MSMA), was bonded onto colloidal silica first, and then mixed with WPU-AC to form a precursor solution. This precursor was spin coated, dried and UV-cured to generate the hybrid films. The silica content in the hybrid thin films was varied from 0 to 30 wt%. Experimental results showed the aggregation of silica particles in the hybrid films. Thus, the silica domain in the hybrid films was varied from 30 to 50 nm by the different ratios of MSMA-silica to WPU-AC. The prepared hybrid films from the crosslinked WPU-AC/MSMA-silica showed much better thermal stability and mechanical properties than pure WPU-AC.

Keywords: *polymer composites, acrylate-modified waterborne polyurethane (WPU-AC), 3-(trimethoxysilyl)propyl methacrylate (MSMA), WPU-AC/MSMA-silica hybrid*

1. Introduction

Organic-inorganic hybrid materials have been extensively studied recently since these materials exhibit the combined characteristics of organic polymer (e.g., flexibility, ductility, dielectric property) and inorganic materials (e.g., rigidity, high thermal stability, strength, hardness, high refractive index) [1–7]. The properties of hybrid materials could be tailored through the adjustment of functionality or segment size of each component. Some special or novel properties can be acquired because of the effects of nanoparticles. Therefore, these materials could be widely used in the applications of protective coatings [8], high refractive index films [9–12], thin film transistor [13], light-emitting diodes [14–16], solar cell [17], optical waveguides materials [18–19], and photochromic materials [20].

Reinforcing of polymer is usually achieved in polymer composites by adding reinforcement such as fibers and particles to the polymer matrix, and some interesting results have been reported using polymer-clay nanocomposites [21], polymer-polyhedral oligomeric silsesquioxane nanocomposites [22], and organic-inorganic hybrids [1–20]. Generally, there are two typical kinds of organic-inorganic nanocomposites. One is the physical blend wherein weak physical interactions exist between organic and inorganic phases, e.g., hydrogen bonding, van der Waals forces. The other possesses strong chemical covalent or ionic bond between organic and inorganic phases. The addition of silica causes increase of crystallinity and chain orientation of polyurethane (PU) due to interactions between polymer and hydroxy groups present on the silica surface [23].

---
*Corresponding author, e-mail: yangch@nuk.edu.tw

The organic-inorganic hybrid method has attracted increasing attention in obtaining high performance composites. This approach has an advantage of processing at relatively low temperature by using a sol-gel process [5, 9, 18].

One of the recently studied materials is PU/inorganic oxide. PU has been used in optical devices due to its good optical properties and processibility. However, its thermal and mechanical properties have limited its applications [21]. One possible solution to the above problems is to hybridize with inorganic oxides such as silica or titania. The commonly used polymer was solvent-based polyurethane, and the silica network in the hybrid materials reported previously was prepared from alkoxysilanes [24]. The size distribution of the inorganic segment in the hybrid materials has not been well controlled, which may be very important for specific optical applications. One possible solution is to use monodispersed colloidal silica instead of preparing silica network from alkoxysilanes [24]. In real hybrid preparation, a selection of optimal hydrolytic media like alkoxysilanes is allowed to control the process of hybrid composites synthesis at an adequate level. However, the preparation of waterborne polyurethane/nanoscale colloidal silica composite films has not been addressed in the past studies. Such composite films could have important applications for optical coating or refractive index tuning films. In our previous work [25], waterborne polyurethane (WPU) was synthesized and followed by adding colloidal silica to prepare WPU-silica hybrids. The silica content in the hybrid thin films was varied from 0 to 50 wt%. The effect of interaction between silica particle and urethane polymer chains is more significant with increasing silica content. The prepared hybrid films show much better thermal stability and mechanical properties than pure WPU. The optical transparence did not linearly decrease with increasing the silica fraction in the hybrid thin film. Results showed that the prepared hybrid films demonstrated tunable transparence with the silica fraction in the films. This belongs to the physical blending. Here, we try to study the characteristics of the chemical covalent bonding/cross-linking through WPU-incorporating monodispersed colloidal silica with a coupling agent.

In this work, we extend our study that the hybrid films of polyester-based waterborne polyurethane incorporating monodispersed colloidal silica with a coupling agent (3-(trimethoxysilyl)propyl methacrylate, MSMA) as reinforcement are employed to investigate their properties. This combines the methods of a sol-gel process, spin coating, and UV-curing polymerization. The characteristics of hybrid films are investigated as a function of colloidal MSMA-silica content.

2. Experimental
2.1. Materials
Ester-type polyol (PA4210, M.W. ≒ 650, Taichin co., Kaohsiung, Taiwan), produced by the transesterification of ethyl glycol (EG), butyl glycol (BG), and adipic acid (mole ratio of EG to BG is 1:1), was dried and degassed under vacuum at 85°C for 24 h. Acetone was distilled over anhydrous $MgSO_4$ (Merck, Germany) at low pressure and stored over 3Å molecular sieve before use. 3-(Trimethoxysilyl)propylmethacrylate (MSMA, 98%, Aldrich, USA), colloidal silica (15–20 nm, 20 wt% in H_2O, Nissan Chem. Ind., Japan), 2-Hydroxyethylacrylate (2-HEA, First Chem., Taiwan), Photoinitiator (Irgacure 2959, Ciba-Gagy, Germany), and ethylene glycol ethyl ether (cellosolve, 99.9%, Acros) were used for the preparation of hybrid films.

2.2. Synthesis of Acrylate-modified WPU (WPU-AC)
Acrylate modified waterborne polyurethane (WPU-AC) dispersions were prepared employing our modified acetone process as Figure 1. The segmented prepolymer (polyester-DMPA-PU) used in this study was synthesized by a one-step addition reaction. To a 1000 ml four-necked round bottomed flask complete with an anchor-propeller stirrer 7 cm in length and 2 cm in width, a nitrogen inlet and outlet, and a thermometer, 4,4-methylenebis-(cyclohexyl isocyanate) (H_{12}MDI, Aldrich, USA) (95 g; 0.362 mol) was charged under a nitrogen gas atmosphere, and a solution of polyester polyol (113.87 g; 0.175 mol) and dimethylolpropionic acid/dimethylformamide (DMPA/DMF = 10 g/25 g, Merck, Germany) was then added over a period of 0.5 h under gentle stirring (300 rpm). The mixture was heated at 100°C until the theoretical NCO content of the

Figure 1. The process of acrylate-modified waterborne polyurethane (WPU-AC) dispersions

prepolymer was reached as determined by the di-n-butylamine titration method [26–27]. 2-Hydroxylethylacrylate (2-HEA, 15 g) was then added to react with the above NCO-terminated PU prepolymer. Partial residual NCO-terminated and 2-HEA-terminated PU solution was adjusted to acetone/PU-AC ratio of 2.8 through addition of a suitable amount of acetone. Triethylamine (TEA, 10 g, Merck, Germany), a neutralizing agent, was added immediately to the above solution (PU-AC solid, 243.87 g). The resulting mixture was then heated at 50°C for 3 min, yielding PU-AC anionomers in acetone. The stoichiometric ratio of TEA to COOH was 1.0. Doubly distilled water (500 g) was added to neutralize PU-AC anionomer solution at respective agitation rate and water addition rate of 500 rpm and 2 ml/min. An aqueous dispersion of ~33 wt% WPU-AC solids was obtained upon removal of acetone by rotary vacuum evaporation.

2.3. Preparation of colloidal MSMA-SiO$_2$

Preparation of colloidal MSMA-SiO$_2$ solution is shown in Figure 2. 3-(Trimethoxysilyl)propyl-methacrylate, aqueous colloidal silica, de-ionized water and ethylene glycol ethyl ether (cellosolve, as

Figure 2. Preparation of MSMA-SiO$_2$ colloidal solution

a solvent) were mixed at the ratio of 2 : 5 : 2 : 25 with adding one drop of acetic acid. Then, the reaction mixture was poured into a three-necked reactor to perform the hydrolysis/condensation reaction. The reaction temperature was maintained at 60°C and the solution was stirred under a nitrogen flow for 2 h to obtain the transparent colloidal MSMA-SiO$_2$.

2.4. Preparation of WPU-AC-MSMA-SiO$_2$ hybrid films

The colloidal MSMA-silica obtained in the procedure of section 2.3. was subsequently mixed with a homogeneous WPU-AC dispersion with a desire ratio of WPU-AC/MSMA-SiO$_2$ and the photoinitiator, 5 wt% for total solid, to perform the preparation of film. The mixed solution was thoroughly stirred for 10 min. Then, this solution was spin coated on a 6 inches silicon wafer to control the final film thickness about 0.5 mm. The coated film was dried in glove box at room temperature (25°C) for 24 h, and then cured on a hot plate at 70°C for 1 h, 90°C for 1 h, and 150°C for 1 h, respectively. Finally, this dried film was subjected to UV-curing (Anly, APT-6S, Taiwan) with the irradiation of 2200 W power for 10 min.

2.5. Characterization

IR spectra of the prepared films were obtained on a KBr pellet using a Nicolet FTIR 550 Fourier-transform IR spectrophotometer. The ^{13}C and ^{29}Si NMR spectra of the solid-state hybrids were determined (Bruker, AVANCE-400, USA) with cross polarization combined with the magic angle spinning (CP/MAS) technique using 200–300 mg samples. The ^{13}C measured conditions of pulse width, recycle delay, contact time and number of scans are 5.5 μs, 5 s, 1000 μs, and 1486 cycles, respectively, at 100.6 MHz. These conditions corresponding to ^{29}Si are 3 μs, 200 s, 1000 μs, and 294 cycles, respectively, at 79.4 MHz. MSMA-SiO$_2$ particle size was measured on the transmittance electron microscope (120 kV, TEM, JOEL JEM-1230, Japan). The fracture surface of hybrid thin films was examined on the (Philips, XL-40FEG, Netherland) field emission scanning electron microscope (SEM).

Thermogravimetric analysis (TGA) was performed under a dry nitrogen flow using a Perkin-Elmer (TGA 7, USA) over a temperature range of 50–800°C at a heating rate 10°C/min. The TGA and DSC samples were prepared by spin-coating the mixed solution on a glass substrate, followed by curing at different temperature steps as described in the film prepared. Differential scanning calorimeter (DSC, Perkin-Elmer, DSC 7, USA) was used for the investigation of glass transition temperature of synthesized hybrid materials. Appropriate 5 mg of samples were sealed in aluminum sample pans. DSC analyses of these hybrid materials were then conducted under nitrogen flow at a heating rate of 20°C/min from –60 to 50°C. The stress-strain properties of the prepared films (1 mm thickness) were tested using an Instron (Shimadzu, AG-IS, Japan) at a pull rate of 10 mm/min.

Wide angle X-ray diffraction measurement was carried out with Rigaku ZD3609N (Japan) series, using CuK$_\alpha$ radiation at a scan rate of 5/min. The transmittance of the prepared hybrid films (ca. 0.5 mm thickness) was peeled from silicone wafer and then measured by using the UV-Vis spectrophotometer (Perkin-Elmer, Lambda 25, USA). The hardness of hybrid films (ca. 0.5 mm thickness) on silicone wafer was measured by using a pencil hardness tester (Jiin-Liang Co., B-3084T4, Taiwan) following the standard method of ASTM D1474-98 (2002).

3. Results and discussion

3.1. Analysis of chemical structure

Figure 3 shows the FTIR spectra of (a) MSMA, (b) colloidal silica, and (c) MSMA-silica (MSMA-SiO$_2$, MSMA/silica = 2.0/1.0), respectively. There are two characteristics from the comparison of the spectra. The first comes from the comparison of the Si–OH absorption band in the spectra. The Si–OH of the pure colloidal silica and MSMA is observed at 963 and 919 cm^{-1}, respectively, which is similar to previous report [28]. However, the Si–OH peak on silica and MSMA is completely disappeared with bonding MSMA onto silica. This suggests the complete condensation of the Si–OH bond on the colloidal silica or bond on MSMA. But a very weak Si–OCH$_3$ peak (1170 cm^{-1}) on MSMA still appeared in the spectrum of MSMA-SiO$_2$. This incomplete condensation of the Si–OCH$_3$ bond in MSMA probably resulted from a high MSMA content and thus the silica could not react with all of the Si–OCH$_3$ bonds on MSMA molecules. The second feature is the narrow absorption band of C=C at 1635 cm^{-1} in the spectra of (a) and (c), but it is reasonably absent in
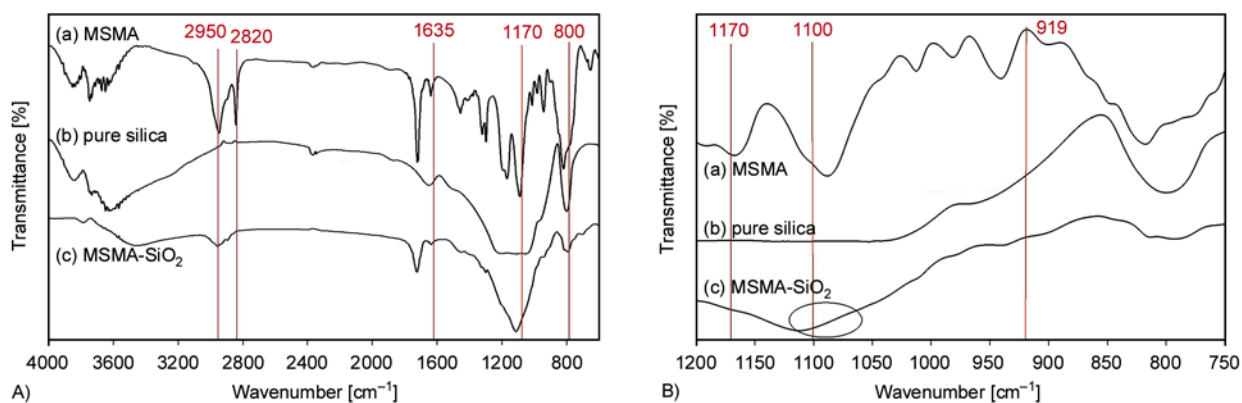
Figure 3. (A) Full-range and (B) specified-range (750–1200 cm^{-1}) FT-IR spectra of (a) MSMA, (b) pure silica and (c) MSMA-SiO$_2$

the spectra (b) of colloidal silica. On the other hand, the absorption bands of asymmetrical Si–O–Si (1110 cm^{-1}) and symmetrical Si–O–Si (800 cm^{-1}) are more significant in the spectrum of MSMA-SiO$_2$. This reflects that the Si–OCH3 groups on MSMA reacted with Si-OH groups on silica through the hydrolysis/condensation, resulting in the formation of Si–O–Si covalent bonding. The characteristic bands of MSMA are observed at 1100–1200, 1735, 2950 and 2800, and 1635 cm^{-1} corresponding to Si–O–C, C=O, –CH$_3$, and C=C, respectively. Figure 4A shows the FTIR spectra of (a) WPU-AC, (b) 5% MSMA-SiO$_2$/WPU-AC and (c) 20% MSMA-SiO$_2$/WPU-AC without UV-curing films, respectively. The absorption bands of C–O–C or Si–O–Si, C=C, C–H, and N–H are observed at 1039–1192, 1635, 2940, and 3250–3500 cm^{-1}, respectively. Asymmetrical Si–O–Si absorption band located at 1100 cm^{-1}, which increases with increasing MSMA-SiO$_2$ content. This indicates the formation of silica structure in the hybrid films. With the increase of MSMA-SiO$_2$ content, the

absorption band of 800 cm^{-1} is also significant, corresponding to the formation of silica network. Moreover, the active group (C=C) at 1635 cm^{-1} still occurs in these films, which serves as further UV-curing polymerization to form an inorganic/organic hybrid film. The FTIR spectra corresponding to these hybrid films after UV-curing are shown in Figure 4B. It is obvious that the absorption band of C=C (1635 cm^{-1}) has disappeared through UV-curing reaction in the hybrid films. Also note that the broad bands of N–H can still be observed in the hybrid films.

^{13}C CP/MAS spectra of the MSMA-SiO$_2$, 5% MSMA-SiO$_2$/WPU-AC, and 20% MSMA-SiO$_2$/WPU-AC with UV-curing is shown in Figure 5. These spectra show a weak absorption peak at 106 ppm. The band might be due to the carbon atom of the Si–OCH$_3$ group [29]. The result indicates that the Si–OCH$_3$ residue exists in MSMA-SiO$_2$, 5% MSMA-SiO$_2$/WPU-AC and 20% MSMA-SiO$_2$/WPU-AC hybrids. For the case of MSMA-SiO$_2$, the carbon atoms on the methyl and methylene groups
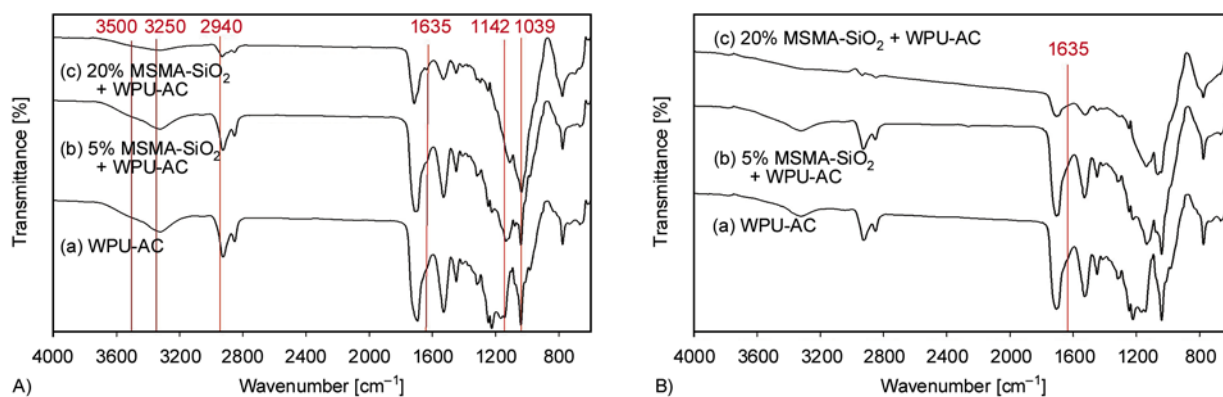
Figure 4. FT-IR spectra (A) before UV-curing and (B) after UV-curing for (a) WPU-AC, (b) 5% MSMA-SiO$_2$/WPU-AC and (c) 20% MSMA-SiO$_2$/WPU-AC
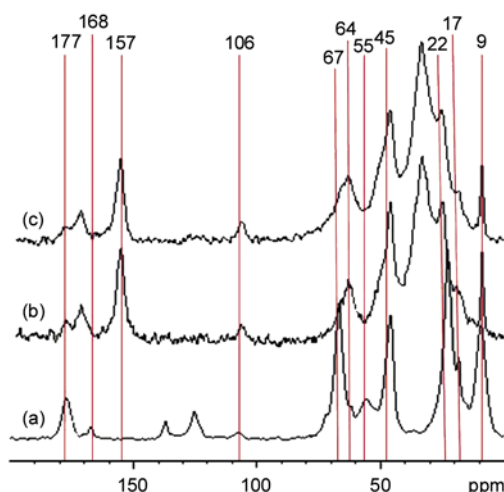
Figure 5. ^{13}C CP/MAS NMR spectra of MSMA-SiO$_2$ and MSMA-SiO$_2$/WPU-AC. (a) MSMA-SiO$_2$, (b) before UV-curing and (c) after UV-curing 5% MSMA-SiO$_2$/WPU-AC.

are observed at 9, 17, 22, 45, 55, 67, 106, 168, and 177 ppm. The absorption of 168 ppm corresponds to the C=C bond. The absorption peaks at 9, 22, and 67 correspond to propyl carbon atoms on MSMA molecules. The band at 17 is the methyl group. The absorption peaks of 45 and 55 ppm correspond to the carbon atoms of acrylic groups. And, the band of 177 ppm arises from the carbon atom of carboxyl group. In addition, the absorption peaks of 125 and 137 ppm result from the residue of cellosolve because this MSMA-SiO$_2$ sample is dried in room temperature. The carbon atoms on the WPU-AC chains are observed at 9, 27, 34, 47, 64, 157, 173 and 177 ppm. A peak centered at 157 ppm, is observed in the carbonyl region consisting of the urea and urethane carbons. The resonance at 64 ppm is ascribed to the soft-segment carbons that are adjacent to a urethane linkage. The absorption bands of 55 and 67 ppm for MSMA-SiO$_2$ are merged into the soft-segment carbons. The peak at 47 ppm is attributed to the secondary carbons on the cyclohexyl rings bonded to nitrogen atoms and CH$_2$ groups (C$_8$), respectively. The peaks at 34 and 27 ppm are associated with the primary carbons in the cyclohexyl rings. It is interesting to note that the line width of the 34 ppm peak

is markedly sharp as compared with other peaks. This feature implies that an effective motional narrowing undergoes possibly due to the segmental motion of polymer chain. In addition, the band of 177 ppm in MSMA-SiO$_2$/WPU-AC becomes weaker than MSMA-SiO$_2$, indicating a diluted effect. The bands of 125 and 137 ppm disappeared in the spectra of MSMA-SiO$_2$/WPU-AC samples. This can be explained that the cellosolve residue is evolved during the baking step at 150°C for 1 h. It is noteworthy that the 168 ppm band of C=C bond exists in both MSMA-SiO$_2$ and MSMA-SiO$_2$/WPU-AC samples. But this peak cannot be observed in MSMA-SiO$_2$/WPU-AC film after UV-irradiation, indicating that the polymerization has been achieved between WPU-AC and MSMA-SiO$_2$ molecules. This result is consistent with FTIR observation.

To gain more insight into the influence of WPU-AC polymer chain on the silica, ^{29}Si CP/MAS NMR experiments of the prepared hybrid films have been performed and shown in Figure 6. The spectra show six peaks at –50 to –51, –57 to –59, –65 to –67, –91 to –93, –100 to –102, and –109 to –111 ppm (Figure 6A), which are assigned to T^1, T^2, T^3, Q^2, Q^3, and Q^4, respectively. The positions of these peaks are similar to previous reports [29, 30]. These peaks correspond to the chemical structures shown in Figure 6B. It is clear that T^i and Q^i peaks come from the coupling agent (MSMA) and colloidal silica, respectively. Q^i and T^i subpeaks were deconvoluted using a curve-fitting method (Figure 6C). The positions of T^1 (–50.5 ppm), T^2 (–58 ppm), T^3 (–66 ppm), Q^2 (–92 ppm), Q^3 (–101 ppm), and Q^4 (–110 ppm) points were first fixed, and then adjusted the area of these subpeaks to fit the corresponding full area of Q^i and T^i subpeaks. The maximum error associated with the deconvolution of ^{29}Si spectra is expected to be ±3%. The degree of condensation (D$_c$) in the hybrid materials was determined by a quantitative analysis based on the peak areas of species. The D$_c$ of the hybrid materials was obtained from the proportion of T^i and Q^i according to Equation (1) [30]:

$$D_c [\%] = \left[\frac{T^1 + 2T^2 + 3T^3}{3} + \frac{Q^1 + 2Q^2 + 3Q^3 + 4Q^4}{4} \right] \cdot 100 \tag{1}$$
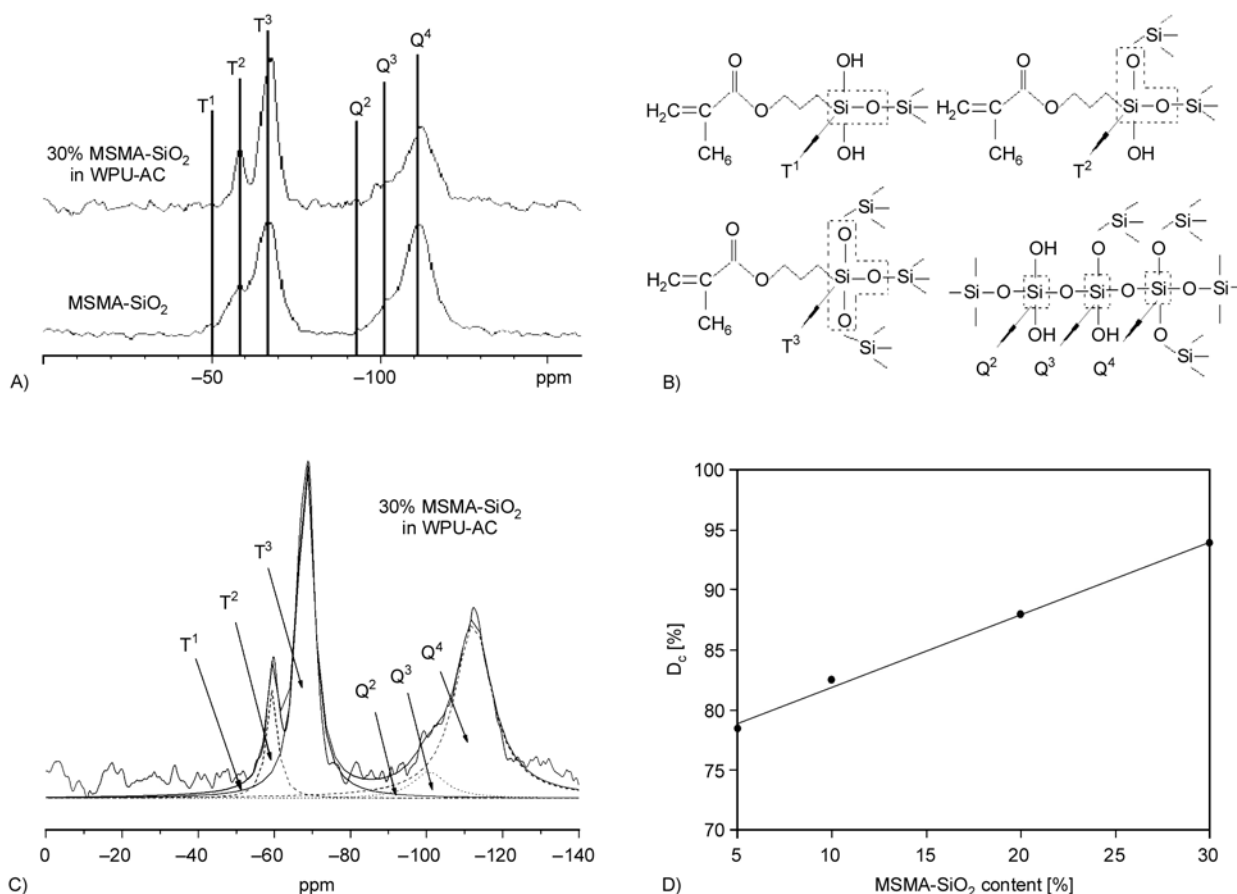
Figure 6. ^{29}Si CP/MAS NMR spectra of the hybrids with different MSMA-SiO$_2$ content: (A) wide scan, (B) theoretical structure, (C) deconvolution of T^1, T^2, T^3, Q^2, Q^3 and Q^4 components, and (D) the degree of condensation (D$_c$) of various MSMA-SiO$_2$ content in the hybrids

The proportion of T^i species decreases with increasing silica content in the prepared hybrid films but that of Q^i species and D$_c$ shows the opposite trend from Figure 6D. Q^i directly depends on the Si–OH condensation of the silica. Hence, it is conceivable that it increases with increasing the silica content. Similar explanation can be used for the D$_c$ because Q^i peaks corresponding to colloidal silica, whereas the weighting and power numbers of Q^i proportions are higher than T^i species (see Equation (1)). In comparison to our previous work [25], there exist significant differences in the ^{29}Si CP/MAS NMR results between the system in this work and the hybrid films of WPU and colloidal silica [25].

3.2. Micro-structure analysis

The size of the silica particle in the hybrid films was estimated from SEM micrographs. The size in the hybrids was generally larger than that in pure MSMA-SiO$_2$ (20–25 nm from TEM image in Figure 7A). It increased to more than 30–50 nm in the

hybrid films of 30% MSMA-SiO$_2$/WPU-AC (Figure 7B). The large size of the silica particle might be due to the incomplete coverage of silica particle surface and results in aggregation. This reflects that the moiety of MSMA-SiO$_2$ plays an important role in the film quality of the prepared hybrid materials. There exists local concave form in the hybrid film in Figure 7B. This might be due to the difference on the thermal expansion coefficient between the WPU-AC and silica.

3.3. Thermal analysis

TGA and DTG curves of the hybrid with 30% are shown in Figure 8A. Notations on Figure 8A are: ΔY is the weight loss due to the thermal degradation of polymer and T_{onset} is the thermal degradation onset temperature for the polymer. Two weight loss points are observed in this TGA curve. Weight loss at 293–316°C (ΔY_1) is due to the degradation of WPU-AC. This process is ascribed to a complex procedure including depolymerization and decom-
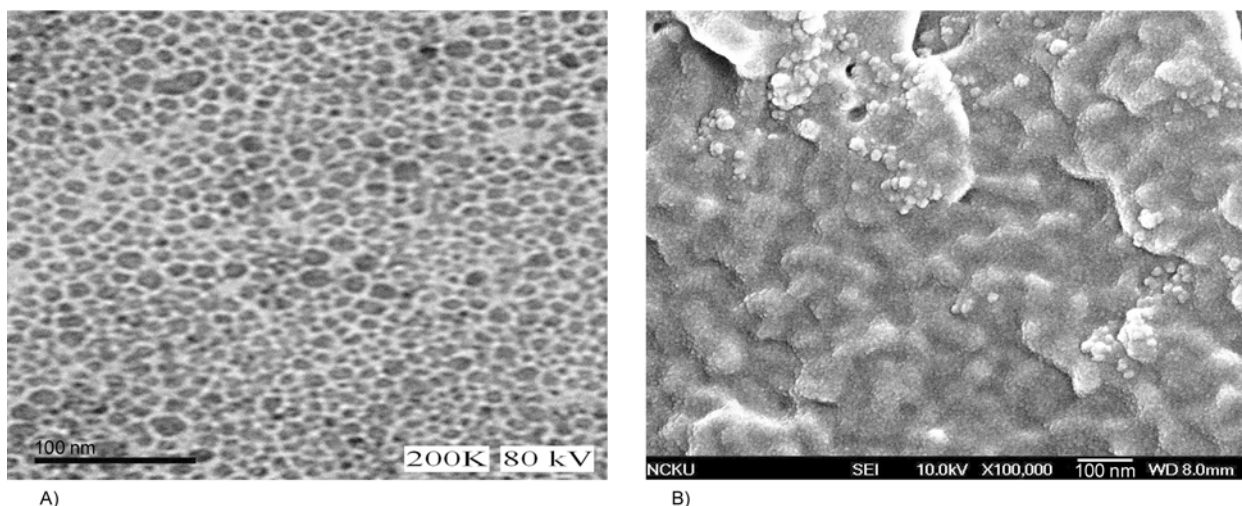
Figure 7. (A) TEM image of MSMA-SiO$_2$ and (B) FE-SEM image of 30% MSMA-SiO$_2$/WPU-AC
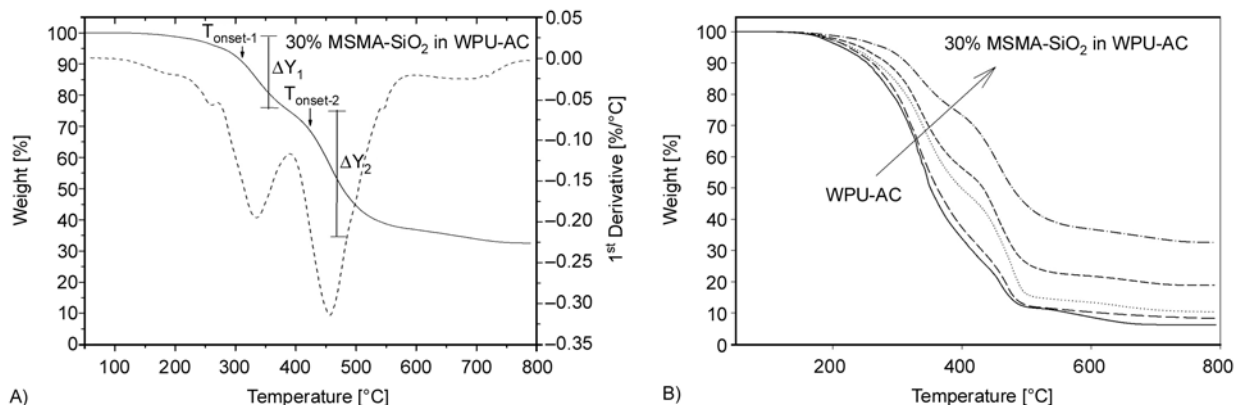
Figure 8. (A) TGA and DTG curves of the hybrid with 30% MSMA-SiO$_2$ in WPU-AC matrix and (B) TGA curve of the hybrids at a heating rate of 10°C/min under nitrogen flow; (—) WPU-AC, (– –) 5% MSMA-SiO$_2$/WPU-AC, (···) 10% MSMA-SiO$_2$/WPU-AC, (---) 20% MSMA-SiO2 /WPU-AC and (– · –) 30% MSMA-SiO$_2$/WPU-AC

position of the urethane and ester units of WPU-AC chains. Meanwhile, ΔY_2 at 427–454°C is due to the generation of delayed-degradation for WPU-AC-MSMA-SiO$_2$ cross-linked networks during the TGA thermal degradation process. Thermal degradation led to the production of aldehyde and alkene end-groups in the molten state. ΔY_1 decreases with increasing the MSMA-SiO$_2$ content, implying that the cross-linked density increases with increasing the MSMA-SiO$_2$ content. This cross-linked network needs higher temperature to decompose. Thus, the materials of higher MSMA-SiO$_2$ content remain more portion of cross-linked networks, resulting in the more MSMA-SiO$_2$ content the higherΔY_2 (Table 1). A shoulder at ca. 240°C may correspond to the degradation of un-reacted components. A series of TGA experiments and the thermal-analysis data of the hybrids are shown in Figure 8B and summarized in Table 1, respectively, revealing that

Table 1. Weight loss and degradation temperature of hybrid films with different MSMA-SiO$_2$ content in WPU-AC

Sample	$T_{onset–1}$ [°C]	$T_{onset–2}$ [°C]	ΔY_1 [%]	ΔY_2 [%]
WPU-AC	293	448	74.2	14.9
5% MSMA-SiO$_2$	301	454	69.8	19.3
10% MSMA-SiO$_2$	307	451	52.0	34.1
20% MSMA-SiO$_2$	310	435	44.9	36.1
30% MSMA-SiO$_2$	316	427	25.4	37.8

$T_{onset–1}$ increases with increasing MSMA-SiO$_2$ content in the hybrids, but ΔY_1 shows the opposite trend. This result is because the chemical bonding between WPU-AC and MSMA-SiO$_2$ increases with increasing MSMA-SiO$_2$ content in the hybrid films, leading to the enhancement of thermal stability by incorporating silica moiety in the hybrids. On the other hand, the second degradation process shows a complex result. The $T_{onset–2}$ first increased and then
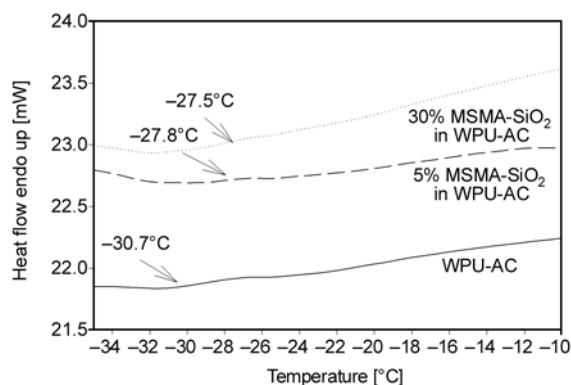
Figure 9. DSC curves of the hybrids with different MSMA-SiO$_2$ content in WPU-AC matrix

decreased with increasing MSMA-SiO$_2$ content in the hybrids. A close examination of ΔY_2 results revealed that this value decreased with increasing MSMA-SiO$_2$ content in the hybrids. This implies that the weight loss involves polymer degradation and silica phase transition.

The glass transition temperatures (T_g) of the hybrids can be carefully measured using DSC instrument. Figure 9 shows the T_g as a function of MSMA-SiO$_2$ content embedded in WPU-AC films after UV-curing. It is clear that the value of T_g increases with increasing MSMA-SiO$_2$ content. This is because the WPU-AC polymer is a linear molecule. With the addition of MSMA-SiO$_2$ in WPU-AC and UV-curing, the chemical bonding is achieved between WPU-AC and MSMA-SiO$_2$ to form a network structure, resulting in an increase in the T_g.

3.4. X-ray diffraction
Figure 10 shows the X-ray diffraction curves for the hybrid samples with varying the MSMA-SiO$_2$ content. For pure WPU-AC, nearly amorphous diffrac-

tion peak is seen near $2\theta = 200$ [31], indicating the crystalline of polyester segments. As the MSMA-SiO$_2$ content increases, the diffraction becomes weaker and broader, whereas this peak gradually shifts to the characteristics of pure silica. This implies that the orientation of polyester segments is significantly disturbed through the addition of MSMA-SiO$_2$ in WPU-AC matrix, suggesting that the influence of the chemical bonding exists between WPU-AC and MSMA-SiO$_2$ after UV-curing. This result is supported by previous FTIR and ^{13}C-NMR results.

3.5. UV-Vis spectra
The transmittance of MSMA-SiO$_2$/WPU-AC hybrid films in the wavelength range of 200–1100 nm is shown in Figure 11, revealing that the transmittance of visible region (633 nm as a criterion) decreases from 92% of pure WPU-AC to 5% of the hybrid with 30% MSMA-SiO$_2$ content. It is because the smaller refractive index of pure silica than the WPU-AC. Hence, the refractive index can be decreased with increasing the MSMA-SiO$_2$ content, whereas the silica particle is isolated as a 'dispersive' heterogeneous phase in the hybrid matrix, which results in a serious light scattering. This leads to a hazy thin film. This is different from the simple WPU-silica hybrid films [25] which the transmittance at 633 nm decreases from 92% of pure WPU to 20% of the hybrid with 20% silica content, and then gradually increases from 20 to 87% of the hybrid with 50% silica content.

Figure 10. X-ray diffractograms of the hybrids with different MSMA-SiO$_2$ content in WPU-AC matrix
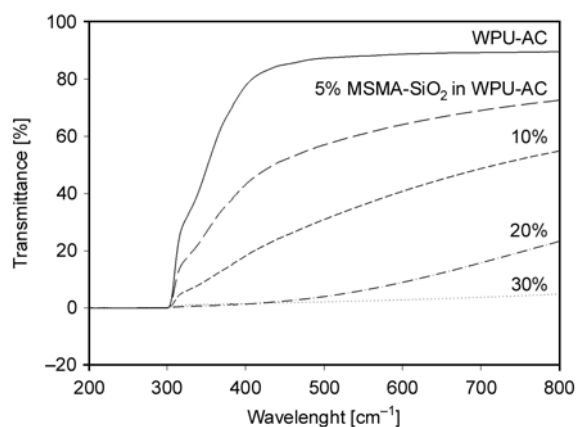
Figure 11. Transmittance variation of the MSMA-SiO$_2$/WPU-AC hybrid films (ca. 0.5 mm thickness) with different MSMA-SiO$_2$ content in the wavelength range of 200–1100 nm

3.6. Mechanical properties

The hardness of the prepared hybrid films was tested by a pencil test, as shown in Table 2. The hardness increases up to 4H with increasing the MSMA-SiO$_2$ content to 10 and more to 30%. It suggests the importance of incorporating the silica moiety on the mechanical properties. The mechanical properties of the hybrid films were obtained from stress-strain experiments. Figure 12 shows the variation of the Young's modulus as a function of the MSMA-SiO$_2$ content for the hybrids. There is a noticeable increase in the Young's modulus with the UV-curing, whereas the Young's modulus of the hybrid films increases with increasing MSMA-SiO$_2$ content. Evidently, the incorporation of MSMA-SiO$_2$ in WPU-AC polymer chains produces a network structure through the UV-curable cross-linking, leading to a significant improvement in the mechanical properties which is in agreement with the FTIR and NMR results. The mechanical strength of the UV-cured WPU-AC incorporating MSMA-SiO$_2$ films is higher than that of the simple WPU-silica hybrid films [25]. Also note that the plateau strength seems to be reached at 20% MSMA-SiO$_2$ content, reflecting that the aggregation of silica particles becomes more significant at MSMA-SiO$_2$ content higher than 20% (see Figure 7B). The high incorporation of MSMA-SiO$_2$ (20–30%) in WPU-AC polymer matrix produces a non-homogeneous network after the UV-curable cross-linking, which cannot contribute more enhancement in mechanical strength.

4. Conclusions

Cross-linked hybrid thin films containing nano-size inorganic materials have been prepared from incorporating reaction between acrylate-waterborne polyurethane and colloidal silica-bearing coupling agent. Experimental results show the aggregation of silica particles in the hybrid films. The incorporation of MSMA-SiO$_2$ in WPU-AC polymer chains produces a network structure through the UV-curable cross-linking, leading to a significant improvement in thermal decomposition temperature, hardness, and the mechanical properties (0–20 wt% MSMA-SiO$_2$). The hybrid also demonstrates a tunable transparence with the added silica fraction in the film.

Acknowledgements

Table 2. Hardness of WPU-AC/MSMA-SiO$_2$ hybrid films

Sample	MSMA-SiO$_2$ content in hybrids				
	WPU-AC	5%	10%	20%	30%
before UV-curing	2B	B	B-HB	HB	HB
after UV-curing	H	2H	4H	4H	4H
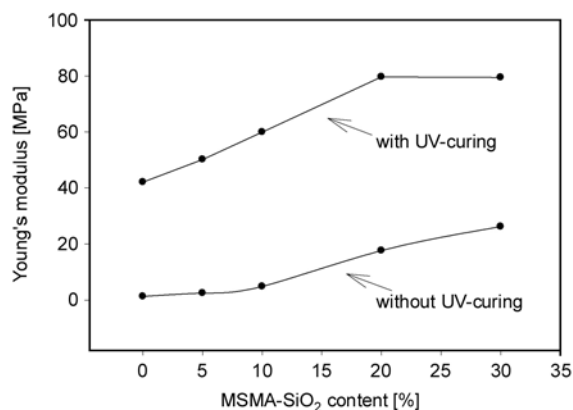
Figure 12. Dependence of the Young's modulus [MPa] on the MSMA-SiO$_2$ content

References
[1] Chten Y., Iroh J. O.: Synthesis and characterization of polyimide/silica hybrid composites. Chemistry of Materials, **11**, 1218–1222 (1999). DOI: 10.1021/cm980428l

[2] Ogoshi T., Itoh H., Kim K-M., Chujo Y.: Synthesis of organic−inorganic polymer hybrids having interpenetrating polymer network structure by formation of ruthenium−bipyridyl complex. Macromolecules, **35**, 334–338 (2002). DOI: 10.1021/ma010819c

[3] Shang X-Y., Zhu Z-K., Yin J., Ma X-D.: Compatibility of soluble polyimide/silica hybrids induced by a coupling agent. Chemistry of Materials, **14**, 71–77 (2002). DOI: 10.1021/cm010088v

[4] Matějka L., Dušek K., Pleštil J., Kříž J., Lednický F.: Formation and structure of the epoxy-silica hybrids. Polymer, **40**, 171–181 (1999). DOI: 10.1016/S0032-3861(98)00214-6

[5] Huang Z. H., Qiu K. Y.: The effects of interactions on the properties of acrylic polymers/silica hybrid materials prepared by the in situ sol-gel process. Polymer, **38**, 521–526 (1997). DOI: 10.1016/S0032-3861(96)00561-7

[6] Yu Y-Y., Chen C-Y., Chen W-C.: Synthesis and characterization of organic–inorganic hybrid thin films from poly(acrylic) and monodispersed colloidal silica. Polymer, **44**, 593–601 (2003). DOI: 10.1016/S0032-3861(02)00824-8

[7] Zhou S., Wu L., Sun J., Shen W.: The change of the properties of acrylic-based polyurethane via addition of nano-silica. Progress in Organic Coatings, **45**, 33–42 (2002).
DOI: 10.1016/S0300-9440(02)00085-1

[8] Ershad-Langroudi A., Mai C., Vigier G., Vassoille R.: Hydrophobic hybrid inorganic-organic thin film prepared by sol-gel process for glass protection and strengthening applications. Journal of Applied Polymer Science, **65**, 2387–2393 (1997).
DOI: 10.1002/(SICI)1097-4628(19970919)65:12<2387::AID-APP11>3.0.CO;2-Z

[9] Wang B., Wilkes G. L., Hedrick J. C., Liptak S. C., McGrath J. E.: New high-refractive-index organic/inorganic hybrid materials from sol-gel processing. Macromolecules, **24**, 3449–3450 (1991).
DOI: 10.1021/ma00011a063

[10] Chen W-C., Lee S-J., Lee L-H., Lin J-L.: Synthesis and characterization of trialkoxysilane-capped poly(methyl methacrylate)–titania hybrid optical thin films. Journal of Materials Chemistry, **9**, 2999–3003 (1999).
DOI: 10.1039/A906157F

[11] Lee L. H., Chen W. C.: High-refractive-index thin films prepared from trialkoxysilane-capped poly(methyl methacrylate)−titania materials. Chemistry of Materials, **13**, 1137–1142 (2001).
DOI: 10.1021/cm000937z

[12] Chang C-C., Chen W-C.: High-refractive-index thin films prepared from aminoalkoxysilane-capped pyromellitic dianhydride–titania hybrid materials. Journal of Polymer Science Part A: Polymer Chemistry, **39**, 3419–3427, (2001).
DOI: 10.1002/pola.1323

[13] Kagan C. R., Mitzi D. B., Dimitrakopoulos C. D.: Organic-inorganic hybrid materials as semiconducting channels in thin-film field-effect transistors. Science, **286**, 945–947 (1999).
DOI: 10.1126/science.286.5441.945

[14] Lee T-W., Park O. O., Yoon J., Kim J-J.: Polymer-layered silicate nanocomposite light-emitting devices. Advanced Materials, **13**, 211–213 (2001).
DOI: 10.1002/1521-4095(200102)13:3<211::AID-ADMA211>3.0.CO;2-H

[15] Huang W. Y., Ho S. W., Kwei T. K., Okamoto Y.: Photoluminescence behavior of poly(quinoline)s in silica glasses via the sol–gel process. Applied Physics Letters, **80**, 1162–1164 (2002).
DOI: 10.1063/1.1450040

[16] Tang J., Wang C., Wang Y., Sun J., Yang B.: An oligophenylenevinylene derivative encapsulatedin sol–gel silica matrix. Journal of Materials Chemistry, **11**, 1370–1373 (2001).
DOI: 10.1039/B009569I

[17] Huynh W. U., Dittmer J. J., Alivisatos A. P.: Hybrid nanorod-polymer solar cells. Science, **295**, 2425–2427 (2002).
DOI: 10.1126/science.1069156

[18] Yoshida M., Prasad P. N.: Sol−gel-processed SiO_2/TiO_2/poly(vinylpyrrolidone) composite materials for optical waveguides. Chemistry of Materials, **8**, 235–241 (1996).
DOI: 10.1021/cm950331o

[19] Xu C., Eldada L., Wu C., Norwood R. A., Shacklette L. W., Yardley J. T., Wei Y.: Photoimageable, low shrinkage organic−inorganic hybrid materials for practical multimode channel waveguides. Chemistry of Materials, **8**, 2701–2703 (1996).
DOI: 10.1021/cm9603009

[20] Biteau J., Chaput F., Lahlil K., Boilot J-P., Tsivgoulis G. M., Lehn J-M., Darracq B., Marois C., Lévy Y.: Large and stable refractive index change in photochromic hybrid materials. Chemistry of Materials, **10**, 1945–1950 (1998).
DOI: 10.1021/cm980106h

[21] Yao K. J., Song M., Hourston D. J., Luo D. Z.: Polymer/layered clay nanocomposites: 2 polyurethane nanocomposites. Polymer, **43**, 1017–1020 (2002).
DOI: 10.1016/S0032-3861(01)00650-4

[22] Jeon H. G., Mather P. T., Haddad T. S.: Shape memory and nanostructure in poly(norbornyl-POSS) copolymers. Polymer International, **49**, 453–457 (2000).
DOI: 10.1002/(SICI)1097-0126(200005)49:5<453::AID-PI332>3.0.CO;2-H

[23] Nunes R. C. R., Pereira R. A., Fonseca J. L. C., Pereira M. R.: X-ray studies on compositions of polyurethane and silica. Polymer Testing, **20**, 707–712 (2001).
DOI: 10.1016/S0142-9418(01)00007-1

[24] Cho J. W., Lee S. H.: Influence of silica on shape memory effect and mechanical properties of polyurethane–silica hybrids. European Polymer Journal, **40**, 1343–1348 (2004).
DOI: 10.1016/j.eurpolymj.2004.01.041

[25] Yang C-H., Liu F-J., Liu Y-P., Liao W-T.: Hybrids of colloidal silica and waterborne polyurethane. Journal of Colloid and Interface Science, **302**, 123–132 (2006).
DOI: 10.1016/j.jcis.2006.06.001

[26] Yang C-H., Lin S-M., Wen T-C.: Application of statistical experimental strategies to the process optimization of waterborne polyurethane. Polymer Engineering and Science, **35**, 722–730 (1995).
DOI: 10.1002/pen.760350812

[27] Wen T-C., Wu M-S., Yang C-H.: Spectroscopic investigations of poly(oxypropylene)glycol-based waterborne polyurethane doped with lithium perchlorate. Macromolecules, **32**, 2712–2720 (1999).
DOI: 10.1021/ma9804489

[28] Chan C-K., Peng S-L., Chu I-M., Ni S-C.: Effects of heat treatment on the properties of poly(methyl methacrylate)/silica hybrid materials prepared by sol–gel process. Polymer, **42**, 4189–4196 (2001). DOI: 10.1016/S0032-3861(00)00817-X

[29] Joseph R., Zhang S., Ford W. T.: Structure and dynamics of a colloidal silica−poly(methyl methacrylate) composite by ^{13}C and ^{29}Si MAS NMR spectroscopy. Macromolecules, **29**, 1305–1312 (1996). DOI: 10.1021/ma951111z

[30] Chang T. C., Wang Y. T., Hong Y. S., Chiu Y. S.: Organic–inorganic hybrid materials. V. Dynamics and degradation of poly(methyl methacrylate) silica hybrids. Journal of Polymer Science Part A: Polymer Chemistry, **38**, 1972–1980 (2000). DOI: 10.1002/(SICI)1099-0518(20000601)38:11<1972 ::AID-POLA60>3.0.co;2-5

[31] Zhang T., Xi K., Yu X., Gu M., Guo S., Gu B., Wang H.: Synthesis, properties of fullerene-containing polyurethane–urea and its optical limiting absorption. Polymer, **44**, 2647–2654 (2003). DOI: 10.1016/S0032-3861(03)00173-3